The effects of shear deformation and rotary inertia on the electrical analogs of beams and plates for multimodal piezoelectric damping

Alan Luo, Boris Lossouarn, Alper Erturk

Received: 6 September 2023 | Revised: 2 November 2023 | Accepted: 20 November 2023

DOI: 10.1002/cta.3899

ORIGINAL PAPER

WILEY

The effects of shear deformation and rotary inertia on the electrical analogs of beams and plates for multimodal piezoelectric damping

Alan Luo[1] | **Boris Lossouarn**[2] | **Alper Erturk**[1]

[1]G.W. Woodruff School of Mechanical Engineering, Georgia Institute of Technology, Atlanta, Georgia, USA

[2]Laboratoire de Mécanique des Structures et des Systémes Couplés, Conservatoire national des arts et métiers, Paris, France

Correspondence
Boris Lossouarn, Laboratoire de Mécanique des Structures et des Systémes Couplés, Conservatoire national des arts et métiers, 292 rue Saint Martin, Paris, 75003, France.
Email: boris.lossouarn@lecnam.net

Abstract

Analogous electrical networks were previously derived from the Euler–Bernoulli and Kirchhoff–Love theories to represent beams and plates, respectively, for use in multimodal structural vibration damping. However, these networks do not account for shear deformations or rotary inertia, which can result in suboptimal vibration damping performance when used on moderately thick beams and plates. In this paper, we investigate the incorporation of shear deformation and rotary inertia using Timoshenko–Ehrenfest beam theory and Mindlin–Reissner plate theory to develop improved electrical networks that can more accurately represent thick beams and plates. Our findings suggest that the inclusion of shear deformation and rotary inertia can significantly improve the frequency coherence of the electrical networks and multimodal vibration damping for thicker structures. The electrical analogs presented here are of use for various applications, especially to conveniently design complex circuit topologies in fields spanning from vibration attenuation to energy harvesting.

KEYWORDS

electrical networks, electromechanical analogy, multimodal damping, piezoelectric coupling, rotary inertia, shear deformation, vibration control

1 | INTRODUCTION

In the 1940s, MacNeal[1] developed electrical networks that modeled mechanical structures using passive components. These networks were initially used for computing structural responses in beams,[2] plates,[3] stiffened shells,[4] and even entire aerospace structures.[5] The concept of using electrical circuits for vibration damping came later in the 1990s, starting with the unimodal RL shunt proposed by Hagood and von Flotow.[6] Hollkamp[7] further expanded on this topic by connecting multiple RL shunts in parallel, which provided a multimodal damping solution. The use of interconnected piezoelectric transducers to create electrical transmission lines was later developed by dell'Isola et al,[8] which demonstrated one of the first instances of multimodal electromechanical coupling using an electrical mesh that represents a modular truss beam. Later, analogous networks were developed specifically for vibration control, which had demonstrated the most optimal electromechanical coupling effect for broadband damping.[9,10]

Vibration damping through electrical analogs is an effective method for multimodal vibration control of structures. In theory, the network is capable of reproducing the exact modal dynamics of the structures in both spatial and frequency domains. This method of damping has been studied for 1-D longitudinal vibration in bars by Lossouarn.[11] Porfiri[12] derived the electrical analog for a Timoshenko beam but only demonstrated the piezoelectric vibration damping using the simplified Euler–Bernoulli (E–B) analog network for single mode damping. The electrical analog of a piezoelectric beam[13] used in multimodal vibration damping was later developed followed by the electrical analog for a piezoelectric plate.[14] More recently, Darleux[15] developed the analogous network for a curved beam. Presently, we focus on improving the analogous networks for beams and plates, which were derived from the E–B beam theory and Kirchhoff-Love plate theory, respectively.

The E–B beam model and the Timoshenko beam model are two widely used mathematical approaches that describe beam deflection and stress distribution.[16] The E–B beam model assumes slender beams with small deflections, neglecting shear deformation and rotational inertia effects. In contrast, the Timoshenko beam model incorporates shear deformation and rotational inertia, making it suitable for scenarios where these effects are significant. In practical applications such as analyzing railway track vibrations, it has been shown that Timoshenko's beam model leads to higher accuracy in the results for modeling moving loads.[17]

The Mindlin–Reissner (M–R) plate theory extends the principles of beam theory to two-dimensional plate structures.[18] Similar to the Timoshenko beam model, the M–R plate theory accounts for the significant influence of shear forces on plate behavior.

By developing electrical networks from the governing equations of Timoshenko's beam theory in Section 2, and M–R's plate theory in Section 3, we can improve the convergence of natural frequencies of the previously derived electrical analogs for beams and plates considered to be thick and short where classical beam and plate theory fails. Furthermore, by using these analogous networks in piezoelectric damping, we can improve the broadband damping frequency response of thick beams and plates.

In this study, we use numerical simulations to validate of the modifications to the original electrical networks[13,14] and the improvements to the multimodal piezoelectric damping for thick structures. Previous research has extensively employed both experimental and numerical approaches to validate the accuracy of the mathematical models, including rods,[19] beams,[13] plates,[20] and rings.[21] These studies have consistently shown a strong correlation between the results obtained from numerical simulations and experimental data, indicating the reliability and robustness of the numerical modeling technique. Therefore, based on the established track record of previous studies, it is reasonable to assume that the numerical simulations in this research will yield comparable results to those obtained through experimental investigations. The utilization of numerical simulations allows for a cost-effective and efficient analysis, providing valuable data and enabling comprehensive understanding of beam and plate responses.

2 | ANALOGOUS ELECTRICAL NETWORK DEVELOPED FROM TIMOSHENKO–EHRENFEST (T–E) BEAM THEORY

2.1 | Equations of motion

The governing equations of motion for the transverse vibrations of a T–E beam of Young's Modulus E, Poisson ratio ν, cross-sectional area A, and area moment of inertia I_x are given by

$$\begin{aligned} \frac{\partial Q}{\partial x} &= \rho A \frac{\partial^2 w}{\partial t^2}, & Q &= kAG\phi, \\ Q + \frac{\partial M}{\partial x} &= \rho I_x \frac{\partial^2 \theta}{\partial t^2}, & M &= EI_x \frac{\partial \theta}{\partial x}, \\ & & \phi + \theta &= \frac{\partial w}{\partial x} \end{aligned} \tag{1}$$

where w is the transverse deflection, Q is the transverse shear force, M is the bending moment, θ is the slope of the deflection curve when the shear force is neglected, and ϕ is the angle of shear along the neutral axis at the same cross section. The total deflection is the sum of both θ and ϕ. Note that when the angle of shear $\phi = 0$, and the inertial term $I_x = 0$, we recover the equations of motion for the E–B beam. The shear modulus is given as $G = E/(2(1+\nu))$. The constant k is the Timoshenko shear coefficient that accounts for the non-uniform strain along the cross-section of the

beam. This value is typically taken to be $k = 5/6$ for rectangular sections, but other more complex and detailed formulations exist.[22]

Following the same finite difference scheme as previous electrical analog derivations,[13] the discrete set of equations can be written as

$$\begin{aligned} -m\omega^2 W_I &= Q_R - Q_L, & M_I &= K_\theta(\theta_R - \theta_L), \\ -\frac{I}{2}\omega^2\theta_L &= \frac{a}{2}Q_L + M_I - M_L, & Q_L &= \frac{K_w}{2}\left(W_I - W_L - \frac{a}{2}\theta_L\right), \\ -\frac{I}{2}\omega^2\theta_R &= \frac{a}{2}Q_R + M_R - M_I, & Q_R &= \frac{K_w}{2}\left(W_R - W_I - \frac{a}{2}\theta_R\right), \end{aligned} \tag{2}$$

where a represents the length of the unit cell, m represents the mass of the element and replaces the quantity $\rho Aa, I$ represents the rotary inertia of the element and replaces the quantity $\rho I_x a, K_w$ is the transverse shear stiffness replacing kAG/a, and K_θ is the bending stiffness replacing EI_x/a.

2.2 | Designing an analogous electrical network

A direct electromechanical analogy is applied to the discrete set of mechanical equations to convert force or moments and velocities into voltages and currents, respectively. The analogy is summarized in Table 1. Applying the direct electromechanical analogy, the set of discrete electrical equations can be written as

$$\begin{aligned} -L\omega^2 q_{w_I} &= V_{w_L} - V_{w_R}, & C_\theta V_{\theta_I} &= q_{\theta_L} - q_{\theta_R}, \\ -\frac{L_\theta}{2}\omega^2 q_{\theta_L} &= -\frac{\hat{a}}{2}V_{w_L} + V_{\theta_L} - V_{\theta_I}, & \frac{C_w}{2}V_{w_L} &= q_{w_I} - q_{w_L} - \frac{\hat{a}}{2}q_{\theta_L} \\ -\frac{L_\theta}{2}\omega^2 q_{\theta_R} &= -\frac{\hat{a}}{2}V_{w_R} + V_{\theta_I} - V_{\theta_R}, & \frac{C_w}{2}V_{w_R} &= q_{w_R} - q_{w_I} - \frac{\hat{a}}{2}q_{\theta_R} \end{aligned} \tag{3}$$

This set of discrete electrical equations describe the network, shown in Figure 1, that is analogous to the T–E beam. Compared to the original E–B derived beam network,[13] this network includes two additional capacitors $C_w/2$, which account for the shear stiffness, and two inductors $L_\theta/2$ which account for the rotary inertia of the beam.

When considering that this electrical unit cell is assembled in series to other unit cells, this network may be further simplified by combining the edge transformers, $C_w/2$ capacitors, and $L_\theta/2$ inductors, as depicted in Figure 2. For instance, when examining successive unit cells where the $L_\theta/2$ inductors are in shown to be in the same electrical line, we note that they can be combined into a single L_θ inductor. It is only at the boundaries of the network where there needs to be a single $L_\theta/2$ inductor to ensure behavior of the circuit is equivalent to the discrete unit cell model shown in Equation (3). The proposed modified unit cell has been shown to be an adequate solution in the network simplifications for thin rings[21]. The inductance value is doubled, the capacitance value is also doubled, and the transformer ratios are thus combined to become $\hat{a}:1$. The simplified network is shown in Figure 3.

TABLE 1 Summary of the direct electromechanical analogies.

Mechanical variables	Electrical variables
Force (F) or moment (M)	Voltage (V)
Velocity ($\dot{u}$) or ($\dot{\theta}$)	Electrical current (i)
Displacement (u) or (θ)	Electrical charge (q)
Compliance ($1/K_\theta$)	Capacitance (C)
Mass (m) or Inertia (I)	Inductance (L)
Unit cell length (a)	Transformer of ratio ($\hat{a}$)

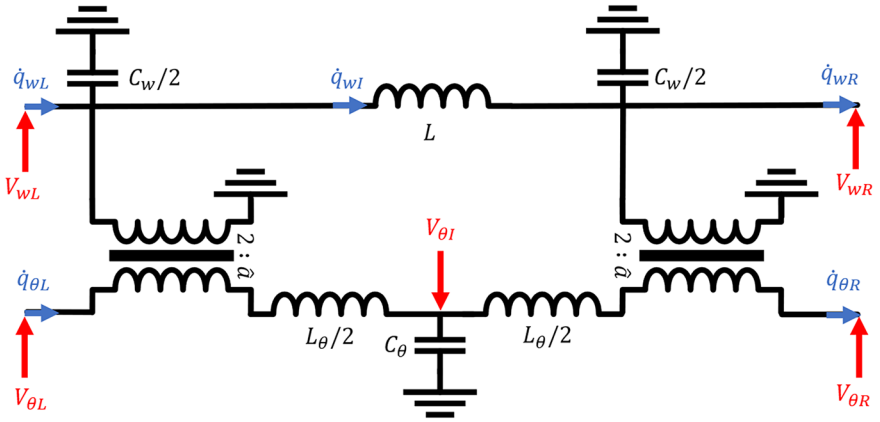

FIGURE 1 Electrical unit cell of the Timoshenko–Ehrenfest Beam that considers shear deformation and rotary inertia.

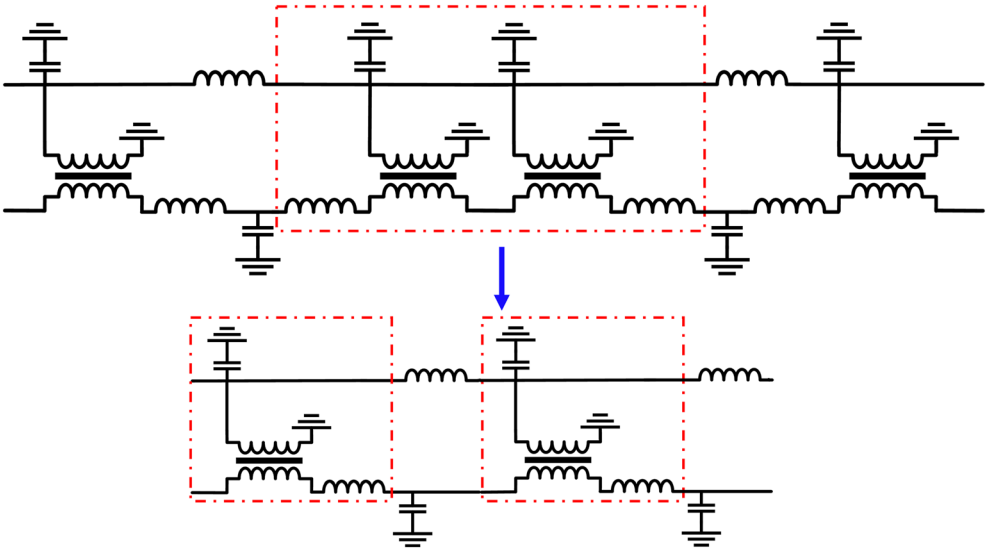

FIGURE 2 Combining the edge electrical components of the unit cell to form a simplified network. The two transformers, two capacitors, and two inductors (-·-·-) are combined into a single transformer, capacitor and inductor.

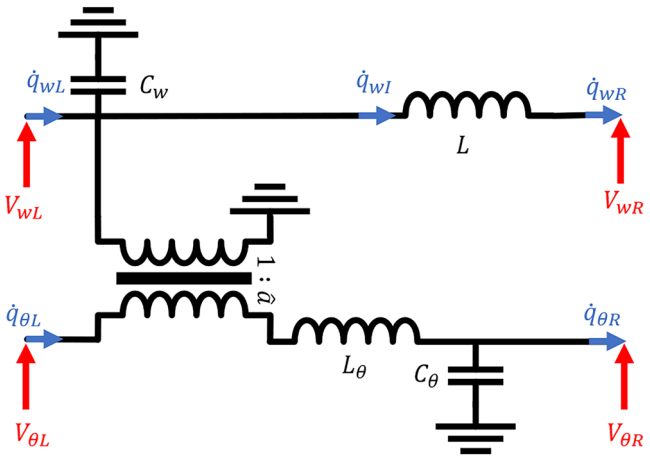

FIGURE 3 Simplified electrical unit cell of the Timoshenko–Ehrenfest Beam that considers shear deformation and rotary inertia.

2.3 | Frequency coherence conditions

Frequency coherence refers to the degree to which the frequencies of mechanical and electrical systems are related. In an electrical network, the natural frequency is determined by the inductance and capacitance in the network. In a mechanical structure, the natural frequency is determined by the mass and stiffness of the structure.

It is not necessary to apply a direct analogy as this does not leave any degree of freedom to optimize the passive component values. Instead, the frequency coherence conditions between the mechanical structure and the electrical network are determined by equating the transfer matrix of each domain to ensure similar dispersion relations.[15] In the mechanical domain, the variables are the displacements, moments, and forces, and in the electrical domain, the variables are currents and voltages. Using nondimensionalized displacements $w^* = w/a$, rotations $\theta^* = \theta$, shear forces $Q^* = aQ/K_\theta$, and bending moments $M^* = M/K_\theta$, the relationships between the left hand terms and right hand terms are given as

$$\begin{pmatrix} w \\ \theta \\ M \\ Q \end{pmatrix}_R^* = \boldsymbol{T}_{\boldsymbol{M}}^* \begin{pmatrix} w \\ \theta \\ M \\ Q \end{pmatrix}_L^* , \quad \begin{pmatrix} q_w \\ q_\theta \\ V_\theta \\ V_w \end{pmatrix}_R^* = \boldsymbol{T}_{\boldsymbol{E}}^* \begin{pmatrix} q_w \\ q_\theta \\ V_\theta \\ V_w \end{pmatrix}_L^* \tag{4}$$

where $\boldsymbol{T}_{\boldsymbol{M}}^*$ refers to the mechanical transfer matrix and $\boldsymbol{T}_{\boldsymbol{E}}^*$ refers to the electrical transfer matrix. Solving the set of discrete equations in Equation (2), we determine the mechanical transfer matrix to be

$$\boldsymbol{T}_{\boldsymbol{M}}^* = \begin{bmatrix} 1-\xi & \frac{\mu}{4}-\frac{\xi}{2} & -\frac{\xi^2}{\gamma}+\frac{2\xi}{\gamma}+\frac{1}{4} & \frac{1}{2} \\ 0 & \frac{\mu}{2}-1 & \frac{1}{2} & 1 \\ -\frac{\gamma}{2} & \mu-\frac{\gamma}{4} & 1-\frac{\xi}{2} & 1 \\ -\gamma & \frac{-\gamma}{2} & 1-\xi & 0 \end{bmatrix} \tag{5}$$

where $\gamma = \frac{ma^2\omega^2}{K_\theta}$, $\mu = \frac{I\omega^2}{K_\theta}$, and $\xi = \frac{m\omega^2}{K_w}$. To ensure frequency coherence conditions, we can equate these ratios to the equivalent electrical ratio using the direct electromechanical analogy resulting in the frequency coherence conditions

$$\frac{K_\theta}{I} = \frac{1}{L_\theta C_\theta}, \quad \frac{K_\theta}{a^2 m} = \frac{1}{\hat{a}^2 L C_\theta}, \quad \frac{K_w}{m} = \frac{1}{L C_w}. \tag{6}$$

with identical dispersion relation and analogous boundary conditions, we retrieve the same natural frequencies from the structure as well as the network.

2.4 | Numerical evaluation of the electrical network

The deflections caused by shear are relatively small for long, slender beams, resulting in minimal differences in such cases. However, if the beams are short and thick, the differences become more significant as shear deflections become more critical. As a result, we consider a simply supported beam on two ends of length $l = 500$ mm, thickness of $h = 50$ mm, width of $b = 17$ mm, and thus, a cross-sectional area of $A = 850$ mm^2. The aluminum beam has a Young's Modulus of $E = 69$ GPa, Poisson's ratio of $\nu = 0.33$, and density of $\rho = 2700$ kg/m^3. The analytical natural frequencies, ω_n for each nth mode, of a T–E beam simply supported on both sides[23] can be determined by solving the expression

$$\omega_n^4 \frac{\rho r^2}{kG} - \omega_n^2 \left(1 + \frac{n^2\pi^2 r^2}{l^2} + \frac{n^2\pi^2 r^2}{l^2}\frac{E}{kG}\right) + \frac{\alpha^2 n^2 \pi^2}{l^4} = 0, \tag{7}$$

where $\alpha^2 = \frac{EI_x}{\rho A}, r^2 = \frac{I_x}{A}$, and the area moment of inertia for a rectangular cross-section is given by $I_x = \frac{1}{12}bh^3$. When solved, the quadratic equation returns two values of ω_n^2 for each nth mode, the lower value corresponding to the bending mode, and the higher value corresponding to the shear deformation mode. It is noted that although the analogous electrical network is capable of reproducing the shear deformation modes, these higher frequency modes fall out of the scope of this paper and thus will not be covered in the analyses.

The simply supported boundary conditions are shown in Table 2 for the beam and its electrical equivalence. The V_w ports remain open circuit while the V_θ ports remain grounded for a simply supported beam.[11] In COMSOL Multiphysics, 100 unit cells of the analogous Timoshenko beam network are assembled to test the validity of the theory. The natural frequencies of the electrical network are then compared with the natural frequencies of an equivalent finite element beam model for a beam. In the finite element simulations, the mesh size used to ensure convergence of the natural frequencies is 5 mm, which is approximately 5% of the size of the shortest wavelength involved in the study. We study four separate cases of the network frequencies compared with the FEM frequencies:

1. The natural frequencies of the E–B beam network.
2. The natural frequencies of the E–B beam network while only considering the addition of rotary inertia.
3. The natural frequencies of the E–B beam network while only considering the addition of shear deformation.
4. The natural frequencies of the T–E beam network which considers both rotary inertia and shear deformation.

The results of the study are shown in Table 3. For a thick beam, it is demonstrated that the E–B beam network is inadequate in representing the natural frequencies, as the error increases with shorter wavelength modes. For lower modes, the E–B theory serves as an adequate approximation.

In the present case, it is also apparent that the impact of the shear deformation on the natural frequencies is far stronger than the impact of the rotary inertia. In the context of the electrical network, the shear deformation refers to the C_w capacitors, and the rotary inertia refers to the L_θ inductors. In the case with only rotary inertia ($C_w = 0$ F), there is still a sizable error for the fifth bending mode. On the other hand, in the case with only shear deformation ($L_\theta = 0$ H), the error for the fifth bending mode decreases significantly. Finally, considering both shear deformation and rotary inertia in the analogous network, otherwise known as the T–E network, we can retrieve almost exactly the same eigenvalues as the FEM eigenvalues.

TABLE 2 Mechanical and electrical boundary conditions for a simply supported beam on both sides.

@$x = 0$ and @$x = L_x$	
Mechanical	**Electrical**
Q, free	V_w, free
$M = 0$	$V_\theta = 0$
$w = 0$	$q_w = 0$
θ, free	q_θ, free

TABLE 3 Natural frequencies of the electrical network with 100 unit cells comparing: FEM frequencies, analytical frequencies, E–B network frequencies, E–B network frequencies with rotary inertia only, E–B network frequencies with shear deformation only, and T–E network frequencies considering both shear deformation and rotary inertia.

FEM	Analytical	E–B network	Rotary inertia	Shear deformation	T–E network
450.77 Hz	450.80 Hz (0.07%)	458.46 Hz (1.65%)	456.55 Hz (1.28%)	452.53 Hz (0.39%)	451.04 Hz (0.06%)
1721.9 Hz	1721.4 Hz (0.03%)	1833.8 Hz (6.33%)	1803.8 Hz (4.82%)	1744.0 Hz (1.34%)	1724.7 Hz (0.22%)
3621.0 Hz	3623.3 Hz (0.06%)	4126.1 Hz (13.4%)	3978.6 Hz (9.88%)	3708.5 Hz (2.42%)	3637.2 Hz (0.45%)
5952.7 Hz	5959.3 Hz (0.11%)	7335.3 Hz (22.4%)	6887.2 Hz (15.70%)	6148.8 Hz (3.29%)	5994.5 Hz (0.70%)
8561.4 Hz	8575.4 Hz (0.16%)	11461.5 Hz (32.6%)	10419.0 Hz (21.70%)	8891.1 Hz (3.85%)	8643.9 Hz (0.96%)

Note: The percent error to the FEM natural frequencies are in parentheses.

2.5 | Piezoelectric vibration damping

We consider a 30-unit cell network coupled to the beam to ensure spatial coherence as well as adequate tuning up to the third mode.[19] The simulation setup is shown in Figure 4. The piezoelectric transducers used are PIC255 square patches with a side length of 15 mm and a thickness of 0.5 mm. The piezoelectric patches replace the C_θ capacitors in the electrical network. The material properties of PIC255 are shown in Table 4. By integrating the surface charge across a piezoelectric patch from a 1 V input voltage, it was determined that the patch capacitance is approximately 4.5 nF. The analogous mass inductor, rotary inertia inductors, and shear capacitors are then determined by the frequency coherence conditions outlined in Equation (6). The optimal resistor placement in series with the transformer, as shown in Figure 5, was derived by Porfiri for simply supported beams[12] and is given by the equation

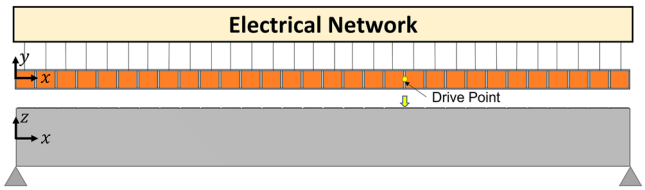

FIGURE 4 Numerical setup of the coupled beam-network. The beam is simply supported on both ends, and the *xy*-plane of the beam is coupled to the electrical network by 30 piezoelectric patches. A drive point measurement, where the measurement and excitation point coincide, is taken for the frequency response.

TABLE 4 Summary of the material properties for the piezoelectric material PIC255.

Compliance (m^2/N)		**Charge constants (m/V)**	
S_{11}^E	1.606×10^{-11}	d_{31}	-1.867×10^{-10}
S_{12}^E	-5.685×10^{-12}	d_{33}	3.996×10^{-10}
S_{13}^E	-7.454×10^{-12}	d_{15}	6.174×10^{-10}
S_{33}^E	1.909×10^{-11}		
S_{44}^E	4.699×10^{-11}		
S_{55}^E	4.699×10^{-11}		
S_{66}^E	5.350×10^{-11}		
Relative permittivity		**Density (kg/m^3)**	
$\epsilon_{11}^\sigma/\epsilon_0$	1852	ρ_p	7800
$\epsilon_{22}^\sigma/\epsilon_0$	1852		
$\epsilon_{33}^\sigma/\epsilon_0$	1751		

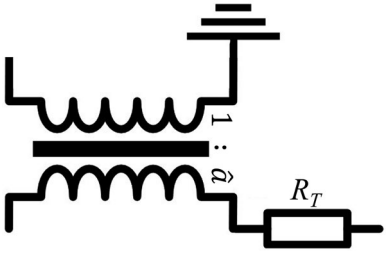

FIGURE 5 Model of the resistor placement in series with the transformer.

$$R_T = k_C \hat{a} \sqrt{\frac{2L}{C_\theta}} \tag{8}$$

where L denotes the inductor that is analogous to the mass term, and C_θ refers to the capacitor analogous to the bending stiffness. The coupling factor is given by $k_C = \sqrt{(\omega_{OC}^2 - \omega_{SC}^2)/\omega_{SC}^2}$, where ω_{OC}^2 refers to the open circuit natural frequency and ω_{OC}^2 refers to the short circuit natural frequency.

The acceleration frequency response of the coupled system subjected to unit force at position $x = 330$ mm is shown in Figure 6. The beam coupled to the T–E network demonstrates adequate tuning with broadband damping across all three modes, whereas coupled to the E–B network, the damping effects are diminished due to poor frequency coherence in the network.

We can conclude that for thick beams, the E–B network is inadequate in optimally attenuating vibrations. Using the T–E network instead results in improved frequency coherence between the electrical and mechanical domains, which subsequently improve the broadband damping of the system. Although there is no consensus on what constitutes a thick beam and thus when to use the T–E network over the E–B network, we can usually switch when the error of the natural frequencies between the mechanical and electrical domains exceed tolerated values.

3 | ANALOGOUS ELECTRICAL NETWORK DEVELOPED FROM M–R PLATE THEORY

3.1 | Equations of motion

M–R extended T–E's beam theory to derive the equations of motions for plates considering shear deformation and rotary inertia. The governing equation of motion for the transverse vibrations of a M–R plate of Young's Modulus E, density ρ, Poisson's ratio ν, side length a, and thickness h is given in terms of the intermediate force and moment quantities by

$$\begin{aligned} \frac{\partial Q_x}{\partial x} + \frac{\partial Q_y}{\partial y} &= \rho h \frac{\partial^2 w}{\partial t^2}, & M &= D\left(\frac{\partial \theta_x}{\partial x} + \frac{\partial \theta_y}{\partial y}\right), \\ Q_x + \frac{\partial M}{\partial x} &= \rho I_x \frac{\partial^2 \theta_x}{\partial t^2}, & Q_x &= kGh\phi_x, \\ Q_y + \frac{\partial M}{\partial y} &= \rho I_y \frac{\partial^2 \theta_y}{\partial t^2}, & Q_y &= kGh\phi_y, \\ & & \phi_x + \theta_x &= \frac{\partial w}{\partial x}, \\ & & \phi_y + \theta_y &= \frac{\partial w}{\partial y}, \end{aligned} \tag{9}$$

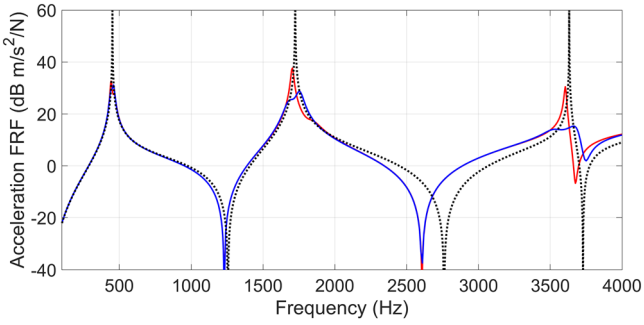

FIGURE 6 Frequency responses of the beam in open circuit configuration (·····), coupled to the Timoshenko–Ehrenfest (T–E) network (——), and coupled to the Euler–Bernoulli (E–B) network (——). The E–B network adequately damps the first mode; however, the vibration mitigation worsens at higher modes due to poor frequency coherence. The T–E network is able to maintain adequate damping for the first three modes.

where w is the transverse deflection, I_x is the second moment of area along the x axis, I_y is the second moment of area along the y axis, and the bending stiffness is given by $D = Eh^3/(12(1-\nu^2))$. Q_x is the transverse shear force in the x direction, Q_y is the transverse shear force in the x direction, and M is the linear combination of the bending moment in both x and y directions, as formulated by Lossouarn.[14] The slopes of the deflection curves when shear forces are neglected in the x direction and y direction are given, respectively, as θ_x and θ_y. The angles of shear along the neutral axis in the x direction and y direction are given, respectively, as ϕ_x and ϕ_y. The total deflection in each direction is the sum of both θ and ϕ. Like the T–E beam theory, when both angle of shear $\phi_x = \phi_y = 0$, and the inertial terms $I_x = I_y = 0$, we recover the equations of motion for the Kirchoff–Love plate. The shear modulus is given as $G = E/(2(1+\nu))$. The constant k is a shear correction factor similar to the Timoshenko shear coefficient in Equation (1). Mindlin chose to use the value $k = \pi^2/12$, whereas Reissner used the value $k = 5/6$. To simplify the problem, we assume that the plate is uniform in thickness and that the unit cells are square. Thus, the rotary inertia in both x and y directions, I_x and I_y, are equivalent and are replaced by the term I.

Substituting the intermediary forces, moments, and displacements into the equilibrium equations yield the equations of motions

$$kGh(\nabla^2 w - \Theta) = \rho h \frac{\partial^2 w}{\partial t^2}, \tag{10a}$$

$$kGh\left(\frac{\partial w}{\partial x} - \theta_x\right) + D\left(\frac{\partial^2 \theta_x}{\partial x^2} + \frac{\partial^2 \theta_y}{\partial x \partial y}\right) = \rho I \frac{\partial^2 \theta_x}{\partial t^2}, \tag{10b}$$

$$kGh\left(\frac{\partial w}{\partial y} - \theta_y\right) + D\left(\frac{\partial^2 \theta_y}{\partial y^2} + \frac{\partial^2 \theta_x}{\partial y \partial x}\right) = \rho I \frac{\partial^2 \theta_y}{\partial t^2}, \tag{10c}$$

where $\nabla^2 = \partial^2/\partial x^2 + \partial^2/\partial y^2$ is the Laplacian operator and $\Theta = \partial \theta_x/\partial x + \partial \theta_y/\partial y$. We can eliminate θ_x and θ_y by differentiating Equations (10b) and (10c) with respect to x and y, respectively, and summing them to obtain the equation

$$D\nabla^2 \Theta + kGh(\nabla^2 w - \Theta) = \rho I \frac{\partial^2 \Theta}{\partial t^2}. \tag{11}$$

Finally, substituting Equation (10a) into (11), we can eliminate Θ and write the single equation of motion in terms of w, given by

$$\left(\nabla^2 - \frac{\rho}{kG}\frac{\partial^2}{\partial t^2}\right)\left(D\nabla^2 - \rho I \frac{\partial^2}{\partial t^2}\right) w + \rho h \frac{\partial^2 w}{\partial t^2} = 0, \tag{12}$$

which confirms the equivalence of the M–R plate equations[18] to Equation (9) which involves the moment variable M.

Using a 2-D finite difference method,[14] the continuous equations of motions in Equation (9) can be rewritten as a set of discrete equations given by

$$\begin{aligned}
-Q_L - Q_B + Q_T + Q_R &= -\omega^2 m W_I, & M_I &= K_\theta(\theta_R - \theta_L + \theta_T - \theta_L),\\
-M_L + M_I + \frac{a}{2}Q_L &= -\omega^2 \frac{m_\theta}{2}\theta_L, & Q_L &= \frac{K_w}{2}\left(W_I - W_L - \frac{a}{2}\theta_L\right),\\
-M_I + M_R + \frac{a}{2}Q_R &= -\omega^2 \frac{m_\theta}{2}\theta_R, & Q_R &= \frac{K_w}{2}\left(W_R - W_I - \frac{a}{2}\theta_R\right),\\
-M_B + M_I + \frac{a}{2}Q_B &= -\omega^2 \frac{m_\theta}{2}\theta_B, & Q_B &= \frac{K_w}{2}\left(W_I - W_B - \frac{a}{2}\theta_B\right),\\
-M_I + M_T + \frac{a}{2}Q_T &= -\omega^2 \frac{m_\theta}{2}\theta_T, & Q_T &= \frac{K_w}{2}\left(W_T - W_I - \frac{a}{2}\theta_T\right),
\end{aligned} \tag{13}$$

where $m = \rho h a$ and $m_\theta = \rho I a$ represent the mass and inertia of the plate element. The second moment of area for a rectangular cross-section per unit cell is given by $I = \frac{1}{12} a h^3$. The bending stiffness is represented by $K_\theta = D$, and the shear stiffness is represented by $K_w = kGh$. In each unit cell, the subscript variables T, L, B, R, I represent the top, left, bottom, right, and center of the cell, respectively.

3.2 | Designing an analogous electrical network

Using the same direct electromechanical analogy from the previous section, the discrete set of mechanical equations can be converted into voltages and currents and are written as

$$\begin{aligned}
V_{w_L} - V_{w_R} + V_{w_B} - V_{w_T} &= -\omega^2 L q_{w_I}, & C_\theta V_{\theta_I} &= q_{\theta_L} - q_{\theta_R} + q_{\theta_B} - q_{\theta_T},\\
V_{\theta_L} - V_{\theta_I} - \frac{a}{2} V_{w_L} &= -\omega^2 \frac{L_\theta}{2} q_{\theta_L}, & \frac{C_w}{2} V_{w_L} &= q_{W_I} - q_{W_L} - \frac{a}{2} q_{\theta_L},\\
V_{\theta_I} - V_{\theta_R} - \frac{a}{2} V_{w_R} &= -\omega^2 \frac{L_\theta}{2} q_{\theta_R}, & \frac{C_w}{2} V_{w_R} &= q_{W_R} - q_{W_I} - \frac{a}{2} q_{\theta_R},\\
V_{\theta_B} - V_{\theta_I} - \frac{a}{2} V_{w_B} &= -\omega^2 \frac{L_\theta}{2} q_{\theta_B}, & \frac{C_w}{2} V_{w_B} &= q_{W_I} - q_{W_B} - \frac{a}{2} q_{\theta_B},\\
V_{\theta_I} - V_{\theta_T} - \frac{a}{2} V_{w_T} &= -\omega^2 \frac{L_\theta}{2} q_{\theta_T}, & \frac{C_w}{2} V_{w_T} &= q_{W_T} - q_{W_I} - \frac{a}{2} q_{\theta_T}.
\end{aligned} \tag{14}$$

The electrical network that corresponds to these discrete electrical equations is shown in Figure 7. Compared with the plate unit cell network derived from Kirchhoff–Love theory, the M–R network consists of four additional capacitors $C_w/2$ that account for the shear stiffness and four additional inductors $L_\theta/2$ that account for the rotary inertia.

Like the beam network, the plate network may be simplified by combining the edge components. The four edge transformers with ratios of $\hat{a}:2$ become two transformers of ratio $\hat{a}:1$, the four shear stiffness capacitors $C_w/2$ become C_w, and the four rotary inertia inductors $L_\theta/2$ become two inductors of value L_θ. The simplified network is shown in Figure 8.

Since the equations for the M–R plate are essentially an extension of the T–E beam in two dimensions coupled by the 1:1 transformer, we can utilize the same frequency coherence conditions.

3.3 | Numerical evaluation of the electrical network

Consider a simply supported rectangular plate on all four sides, with the x side length $l_x = 400$ mm, y side length $l_y = 320$ mm, and a thickness of $h = 50$ mm. The aluminum plate has a Young's modulus of $E = 69$ GPa, Poisson's ratio of $\nu = 0.33$, and density of $\rho = 2700$ kg/m^3. The analytical natural frequencies, ω_n for each (m, n)th mode, of a M–R plate simply supported on all sides[23] can be determined by solving the expression

$$\left(-\frac{m^2\pi^2}{l_x^2} - \frac{n^2\pi^2}{l_y^2} + \frac{\rho\omega_{mn}^2}{kG}\right)\left(-D\left(\frac{m^2\pi^2}{l_x^2} + \frac{n^2\pi^2}{l_y^2}\right) + \frac{\rho h^3 \omega_{mn}^2}{12}\right) - \rho h \omega_{mn}^2 = 0. \tag{15}$$

As in the case with the equation for the natural frequencies of the Timoshenko beam, this quadratic equation returns a lower bending frequency and a higher shear frequency for each (m, n)th mode.

The simply supported boundary conditions are shown in Table 5 for the plate and its electrical equivalence. The numerical setup is shown in Figure 9. In the numerical model, 20 by 16 unit cells of the analogous plate network are assembled to test the validity of the theory. In comparison, the natural frequencies of an equivalent finite element plate are calculated. In the finite element simulations of the plate, the mesh size used to ensure convergence of the natural frequencies is 6.5 mm, which is approximately 5% of the size of the shortest wavelength involved in the study. We study four separate cases of the network frequencies compared to the FEM plate frequencies:

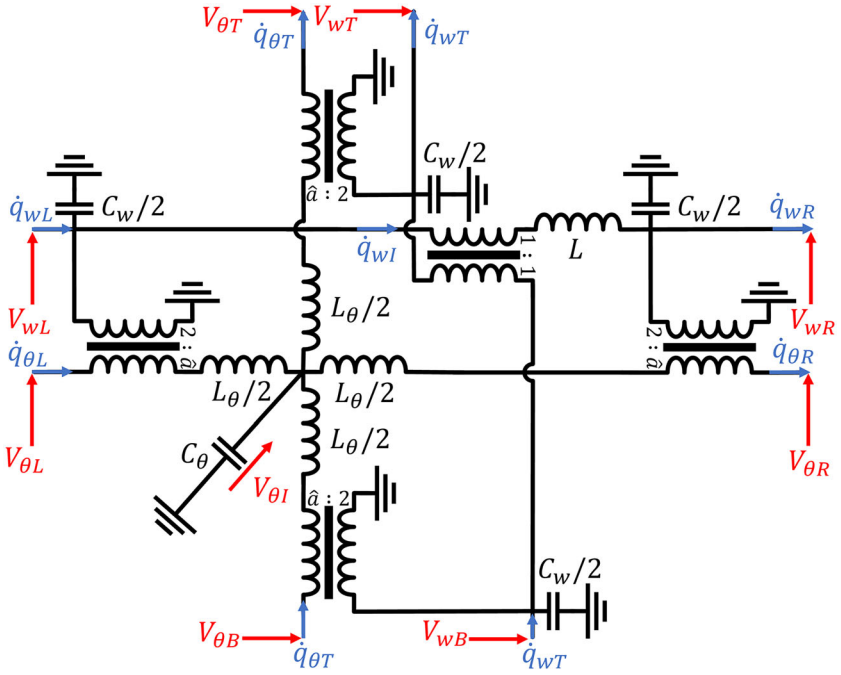

FIGURE 7 Electrical unit cell of the Mindlin–Reissner plate that considers shear deformation and rotary inertia.

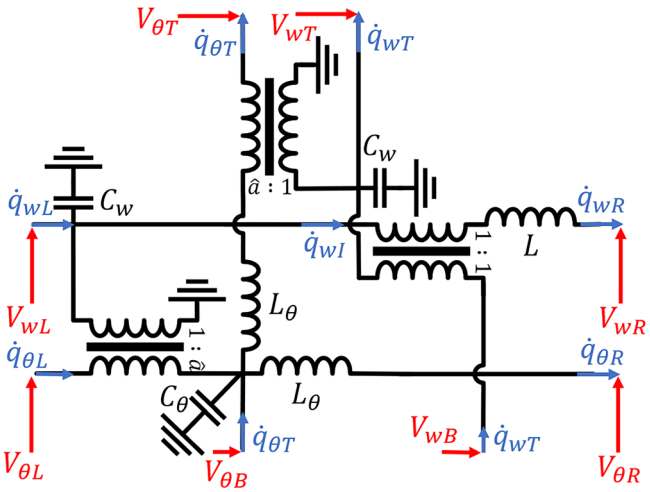

FIGURE 8 Simplified electrical unit cell of the Mindlin–Reissner plate that considers shear deformation and rotary inertia.

1. The natural frequencies of the Kirchoff–Love (K–L) plate network.
2. The natural frequencies of the K–L plate network while only considering the addition of rotary inertia.
3. The natural frequencies of the K–L plate network while only considering the addition of shear deformation.
4. The natural frequencies of the M–R plate network which considers both rotary inertia and shear deformation.

The results of the study are shown in Table 6. Similar to the previous case for the thick beam, for a thick plate, it is demonstrated that the K–L plate network is inadequate in representing the natural frequencies, as the error increases with higher wavelength modes. For lower modes, the K–L theory serves as an adequate approximation.

Similar to the case with the beam, the impact of the shear deformation on the natural frequencies is far stronger than the impact of the rotary inertia for plates. In the case with only rotary inertia ($C_w = 0$ F), there is still a sizable error for the fifth bending mode. On the other hand, in the case with only shear deformation ($L_\theta = 0$ H) for plates, the

TABLE 5 Mechanical and electrical boundary conditions for a simply supported plate.

$@x=0, x=L_x, y=0, y=L_y$	
Mechanical	**Electrical**
Q, free	V_w, free
$M=0$	$V_\theta=0$
$w=0$	$q_w=0$
θ, free	q_θ, free

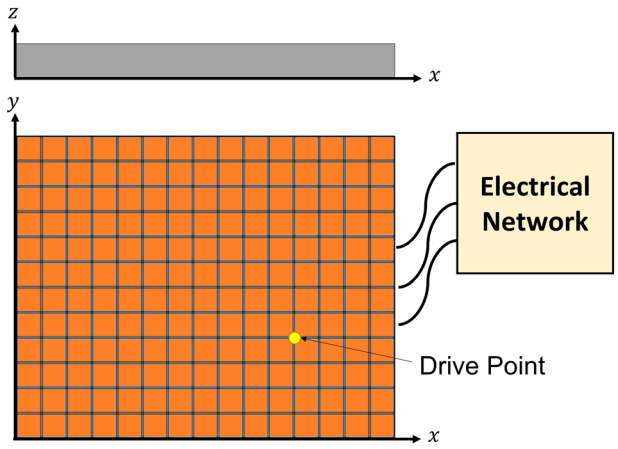

FIGURE 9 Numerical setup of the coupled plate-network. The plate is simply supported on all four sides, and the *xy*-plane of the plate is coupled to the electrical network by an array of 15×12 piezoelectric patches. A drive point measurement, where the measurement and excitation point coincide, is taken for the frequency response.

TABLE 6 Natural frequencies of the electrical network with 20 by 16 unit cells comparing: FEM frequencies, analytical frequencies, K–L network frequencies, K–L network frequencies with rotary inertia only, K–L network frequencies with shear deformation only, and M–R network frequencies considering both shear deformation and rotary inertia.

FEM	Analytical	K–L network	Rotary inertia	Shear deformation	M–R network
1820.43 Hz	1815.29 Hz (0.28%)	1939.21 Hz (6.52%)	1938.56 Hz (6.49%)	1834.31 Hz (0.76%)	1833.83 Hz (0.74%)
3703.19 Hz	3682.95 Hz (0.54%)	4192.53 Hz (13.21%)	4189.48 Hz (13.13%)	3743.38 Hz (1.09%)	3741.69 Hz (1.04%)
4672.57 Hz	4641.87 Hz (0.66%)	5439.52 Hz (16.41%)	5434.51 Hz (16.31%)	4716.71 Hz (0.94%)	4714.26 Hz (0.89%)
6272.83 Hz	6219.98 Hz (0.84%)	7692.82 Hz (22.64%)	7682.76 Hz (22.48%)	6352.12 Hz (1.26%)	6348.27 Hz (1.20%)
6433.80 Hz	6376.31 Hz (0.89%)	7886.22 Hz (22.57%)	7875.65 Hz (22.41%)	6485.93 Hz (0.81%)	6481.96 Hz (0.75%)

Note: The percent error to the FEM plate frequencies are in parentheses.

error is significantly lower, even comparable with the M–R network results. Finally, when considering both the effects of shear deformation and rotary inertia in the analogous network, otherwise known as the M–R network, we can recover almost exactly the same eigenvalues as the FEM eigenvalues with errors around 1%.

3.4 | Piezoelectric vibration damping

We consider a 15 by 12 unit cell network coupled to a thick plate simply supported on all four sides for a study on the effects of the improved network on multimodal piezoelectric damping. The piezoelectric transducers used are PIC255 square patches with a side length of 25 mm and a thickness of 0.5 mm. The patch capacitance is approximately 11.88 nF. Following the same procedure as for the beam, the analogous mass inductor, rotary inductors, and shear capacitors are then determined by the frequency coherence conditions outlined in Equation (6).

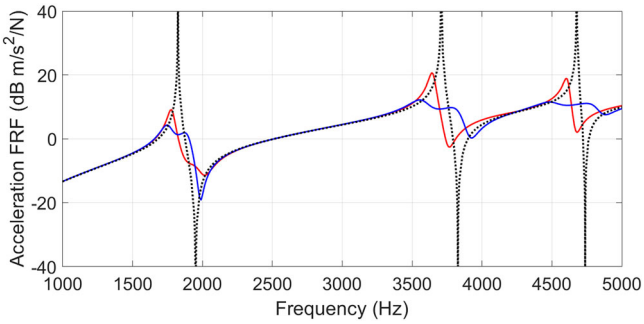

FIGURE 10 Frequency responses of the plate in open circuit configuration (·····), coupled to the Mindlin–Reissner (M–R) network (——), and coupled to the K–L network (——). The vibration mitigation using the K–L network is deteriorated due to the poor frequency coherence; however, the T–E network is able to increase piezoelectric damping.

The plate is excited and measured at the drive point as shown in Figure 9. The measured frequency response function using both the original network and the enhanced network are shown in Figure 10. The frequency response utilizing the enhanced electrical network shows stronger broadband damping than the original network. Although the original network still achieves vibration damping for the three modes shown, the vibration mitigation is lower. The enhanced network is able to create the broadband damping due to the improved frequency coherence.

4 | CONCLUSION

This study addresses the limitations of existing electrical networks derived from E–B and Kirchhoff–Love theories, which fail to account for shear deformations in thick beams and plates. By incorporating T–E beam theory and M–R plate theory, this study aimed to develop enhanced electrical networks capable of accurately representing such structures. The findings of this investigation demonstrated that the inclusion of shear deformation and rotary inertia resulted in significant improvements in frequency coherence and multimodal vibration damping for thicker structures.

The results of this study provide a more comprehensive and accurate representation of the behavior of thick beams and plates. The improved electrical networks derived from the incorporation of shear deformation can enable more effective vibration damping strategies in practical applications. These findings highlight the significance of considering shear deformations when designing damping systems for thick structural elements.

Using numerical simulations, we verified the improvements in the broadband frequency response for thick beams and plates using the enhanced networks that consider shear deformation and rotary inertia. For both structures, although it was shown that the added effect of shear deformation has a more drastic effect on improving the frequency coherence of the network, considering both rotary inertia and shear deformation effects leads to the best frequency coherence with less than 1% error. These may be practical considerations when building the electrical networks. Depending on the application, it may be possible to exclude the rotary inertia if the error is acceptable.

In the frequency response for both structures, we observe that the original electrical networks (E–B and K–L) still provide adequate piezoelectric damping for the first mode, but the vibration mitigation deteriorates for successive modes. On the other hand, the enhanced electrical networks (T–B and M–R) are able to provide adequate damping for multiple modes. These findings highlight the significance of considering shear deformations and rotary inertia when designing analogous electrical network damping systems for thick structural elements.

DATA AVAILABILITY STATEMENT

The data that supports the findings of this study are available from the corresponding author upon reasonable request.

ORCID

Alan Luo https://orcid.org/0000-0002-2266-4786
Boris Lossouarn https://orcid.org/0000-0001-7382-3137
Alper Erturk https://orcid.org/0000-0003-0110-5376

REFERENCES

1. MacNeal RH. The solution of partial differential equations by means of electrical networks. *dissertation (Ph.D.) Thesis*; 1949.
2. Benscoter SU, MacNeal RH. Introduction to electrical-circuit analogies for beam analysis. *Technical Report*; 1952.
3. Benscoter SU, MacNeal RH. Equivalent-plate theory for a straight multicell wing. *Technical Report*; 1952.
4. MacNeal RH. Electrical analogies for stiffened shells with exible rings. *Report*, NACA; 1954.
5. MacNeal RH. *Electric Circuit Analogies for Elastic Structures*, Airplane, missle and spacecraft structure series. John Wiley & Sons Canada, Limited; 1962: 9780471560494. https://books.google.com/books?id=RNC7zQEACAAJ
6. Hagood NW, von Flotow A. Damping of structural vibrations with piezoelectric materials and passive electrical networks. *J Sound Vib*. 1991;146(2):243-268. doi:10.1016/0022-460X(91)90762-9
7. Hollkamp JJ. Multimodal passive vibration suppression with piezoelectric materials and resonant shunts. *J Intell Mater Syst Struct*. 1994; 5(1):49-57. doi:10.1177/1045389X9400500106
8. dell'Isola F, Vidoli S. Continuum modelling of piezoelectromechanical truss beams: an application to vibration damping. *Arch Appl Mech*. 1998;68(1):1-19. doi:10.1007/s004190050142
9. Alessandroni S, dell'Isola F, Porfiri M. A revival of electric analogs for vibrating mechanical systems aimed to their efficient control by PZT actuators. *Int J Solids Struct*. 2002;39(20):5295-5324. doi:10.1016/S0020-7683(02)00402-X
10. dell'Isola F, Porfiri M, Vidoli S. Piezo-electromechanical (PEM) structures: passive vibration control using distributed piezoelectric transducers. *C R Mécanique*. 2003;331(1):69-76. doi:10.1016/S1631-0721(03)00022-6
11. Lossouarn B. Multimodal vibration damping of structures coupled to their analogous piezoelectric networks. *Thesis*; 2016.
12. Porfiri M, dell'Isola F, Frattale Mascioli FM. Circuit analog of a beam and its application to multimodal vibration damping, using piezoelectric transducers. *Int J Circ Theory Appl*. 2004;32(4):167-198. doi:10.1002/cta.273
13. Lossouarn B, Deu J-F, Aucejo M. Multimodal vibration damping of a beam with a periodic array of piezoelectric patches connected to a passive electrical network. *Smart Mater Struct*. 2015;24(11). doi:10.1088/0964-1726/25/11/115042
14. Lossouarn B, Aucejo M, Deu J-F, Cunefare KA. Design of a passive electrical analogue for piezoelectric damping of a plate. *J Intell Mater Syst Struct*. 2018;29(7):1301-1314. doi:10.1177/1045389X17731232
15. Darleux R, Lossouarn B, Giorgio I, dell'Isola F, Deü J-F. Electrical analogs of curved beams and application to piezoelectric network damping. *Math Mech Solids*. 2022;27(4):578-601. doi:10.1177/10812865211027622
16. Labuschagne A, van Rensburg NFJ, van der Merwe AJ. Comparison of linear beam theories. *Math Comput Modell*. 2009;49(1):20-30. doi:10.1016/j.mcm.2008.06.006
17. Zhang X, Thompson D, Sheng X. Differences between Euler–Bernoulli and Timoshenko beam formulations for calculating the effects of moving loads on a periodically supported beam. *J Sound Vib*. 2020;481:115432. doi:10.1016/j.jsv.2020.115432
18. Elishakoff I. *Handbook on Timoshenko–Ehrenfest Beam and Uflyand–Mindlin Plate Theories*. Singapore: World Scientific; 2020.
19. Lossouarn B, Aucejo M, Deü J-F. Multimodal coupling of periodic lattices and application to rod vibration damping with a piezoelectric network. *Smart Mater Struct*. 2015;24(4):45018. doi:10.1088/0964-1726/24/4/045018
20. Lossouarn B, Deü J-F, Aucejo M, Cunefare KA. Multimodal vibration damping of a plate by piezoelectric coupling to its analogous electrical network. *Smart Mater Struct*. 2016;25(11):115042. doi:10.1088/0964-1726/25/11/115042
21. Luo A, Lossouarn B, Erturk A. Analogous piezoelectric network for multimodal vibration attenuation of a thin circular ring. *Smart Mater Struct*. 2023;32:115024. doi:10.1088/1361-665X/ad0139
22. Dong SB, Alpdogan C, Taciroglu E. Much ado about shear correction factors in timoshenko beam theory. *Int J Solids Struct*. 2010;47(13): 1651-1665. doi:10.1016/j.ijsolstr.2010.02.018
23. Shames IH, Dym CL. Energy and finite element methods in structural mechanics. doi:10.1201/9780203757574; 1985.

How to cite this article: Luo A, Lossouarn B, Erturk A. The effects of shear deformation and rotary inertia on the electrical analogs of beams and plates for multimodal piezoelectric damping. *Int J Circ Theor Appl*. 2024; 52(6):2985-2998. doi:10.1002/cta.3899